EMi | Taylor & Francis
Taylor & Francis Group

One HA stalk topping multiple heads as a novel influenza vaccine

Ping Zhou[a,b,#], Tianyi Qiu[c,d#], Xiang Wang[e], Xi Yang[e], Hongyang Shi[a], Caihong Zhu[e], Weiqian Dai[a], Man Xing[a], Xiaoyan Zhang[e], Jianqing Xu[e] and Dongming Zhou[a,e]

[a]Department of Pathogen Biology, School of Basic Medical Sciences, Tianjin Medical University, Tianjin, People's Republic of China; [b]Chinese Academy of Sciences, Institut Pasteur of Shanghai, Shanghai, People's Republic of China; [c]Institute of Clinical Science, ZhongShan Hospital, Fudan University, Shanghai, People's Republic of China; [d]Shanghai Institute of Infectious Disease and Biosecurity, Fudan University, Shanghai, People's Republic of China; [e]Shanghai Public Health Clinical Center, Fudan University, Shanghai, People's Republic of China

ABSTRACT
Classic chimeric hemagglutinin (cHA) was designed to induce immune responses against the conserved stalk domain of HA. However, it is unclear whether combining more than one HA head domain onto one stalk domain is immunogenic and further induce immune responses against influenza viruses. Here, we constructed numerous novel cHAs comprising two or three fuzed head domains from different subtypes grafted onto one stalk domain, designated as cH1-H3, cH1-H7, cH1-H3-H7, and cH1-H7-H3. The three-dimensional structures of these novel cHAs were modelled using bioinformatics simulations. Structural analysis showed that the intact neutralizing epitopes were exposed in cH1-H7 and were predicted to be immunogenic. The immunogenicity of the cHAs constructs was evaluated in mice using a chimpanzee adenoviral vector (AdC68) vaccine platform. The results demonstrated that cH1-H7 expressed by AdC68 (AdC68-cH1-H7) induced the production of high levels of binding antibodies, neutralizing antibodies, and hemagglutinin inhibition antibodies against homologous pandemic H1N1, drifted seasonal H1N1, and H7N9 virus. Moreover, vaccinated mice were fully protected from a lethal challenge with the aforementioned influenza viruses. Hence, cH1-H7 cHAs with potent immunogenicity might be a potential novel vaccine to provide protection against different subtypes of influenza virus.

Introduction

Influenza viruses can cause acute respiratory diseases, leading to severe pneumonia or cardiopulmonary dysfunction, which results in approximately 3–5 million severe infections worldwide annually and 290,000–650,000 cases of respiratory death [1]. With the severe acute respiratory syndrome coronavirus 2 (SARS-CoV-2) outbreak, the influenza virus has gained renewed attention. Numerous studies have shown that the risk of death doubles in patients concomitantly infected with the SARS-CoV-2 and influenza virus [2, 3]. As SARS-CoV-2 cases have decreased, China has experienced a significant increase in cases of influenza, starting from early February 2023. This trend intensified towards the end of February and peaked in mid-March 2023. According to the weekly report on influenza surveillance from the National Influenza Center at China CDC, 5,703 outbreaks of influenza-like illness were reported across China from week 14

in 2022 through week 14 in 2003. Vaccination is the most economical and efficient means of controlling influenza virus infection, while the currently available strain-specific seasonal influenza vaccine has a decreased effectiveness due to the antigenic drift and shift of the virus. The effectiveness of the seasonal influenza vaccine crucially depends on the match between vaccine strains and the circulating influenza virus [4]. Although annual reformulations are performed based on conscientious surveillance and prediction, mismatches of the seasonal influenza vaccine have occurred occasionally in the past, such as in 1997/1998, 2003/2004, 2007/2008, 2012/2013, and 2014/2015 influenza seasons [5, 6], that resulted in dramatic drops in vaccine effectiveness. Furthermore, the production of commonly used trivalent inactivated split vaccines (TIV) relies heavily on the supply of chicken embryos and is time-consuming, making it impossible to respond rapidly to global influenza pandemics.

Therefore, developing a vaccine that induces a broadly cross-protective and durable immunity capable of rapid and large-scale production is urgently needed.

Massive efforts have been undertaken to develop a universal influenza vaccine by eliciting strong immune responses to highly conserved antigens, such as the stalk domain of hemagglutinin (HA), the ectodomain of the M2 ion channel (M2e), and the internal proteins nucleoprotein (NP) and matrix protein (M1) [7, 8]. HA, the primary antigen of the influenza virus, is a homotrimeric glycoprotein present on the virion surface and is composed of a membrane distal globular head domain and a proximal stalk domain [9]. The globular head domain with abundant neutralizing epitopes is immunogenic but frequently undergoes antigenic drift, enabling virus evasion from herd immunity [10]. Compared to the variable head domain, the stalk domain is highly conserved, thereby being an ideal target for a universal influenza vaccine [11]. However, owing to shadowing effects from the globular head domain, the stalk domain is poorly immunogenic. To address this issue and enhance immune responses towards the stalk, a prominent immunogen design known as chimeric HA (cHA) was first developed by Peter Palese, which has been applied to the development of a universal influenza vaccine against the influenza A or influenza B virus [12–14]. Numerous stable cHA candidates could be constructed by combining the HA stalk domain from one influenza virus subtype with an exotic globular head domain, which can induce broadly stalk-reactive antibodies through sequential vaccination regimens. However, due to the weak immunogenicity of the stalk, adjuvant supplementation is indispensable, and sequential immunization schedules could be complicated.

Recombinant virus vector-based vaccines have become an attractive alternative to classical inactivated vaccines for delivering diverse antigens due to their easy manipulation and rapid production. The chimpanzee adenovirus has demonstrated superiority over the widely used vaccine vector adenovirus serotype 5 (AdHu5) due to its lower seroprevalence in humans; thus, the efficacy of a vaccine based on it is barely crippled by the pre-existing immunity. More recently, the efficacious vaccine ChAdOx1 nCoV-19 (AZD1222) based on the chimpanzee adenovirus type Y25 vector (ChAdOX1) has been successfully licensed for combating the worldwide pandemic caused by SARS-CoV-2, which has shown potent immunogenicity and acceptable tolerability in various populations [15, 16]. Moreover, chimpanzee-derived vectors have demonstrated a robust capacity to elicit humoral and cellular responses [17–21], making it a promising and appealing vaccine platform.

Notoriously, HA protein can naturally form stable homotrimers with the help of stalk and the classical cHA design has proved that the conformation of the

heterologous HA head domain in cHA would maintain intact. Several broadly neutralizing antibodies targeting head domains on the trimer such as the interface between two head domains, the interface of three head domains at the trimer apex have recently been isolated [22–25]. Based on it, we adapted HA stalk domain as backbone and innovatively developed a series of novel cHAs. Different from the current classical cHA, cHAs were constructed by combining multiple head domains from different virus subtypes onto one stalk domain to display the influenza HA head in its native-like trimeric conformation and keep the conformation of the antigenic sites as intact as possible to stimulate immune response against multiple subtypes of influenza virus. Moreover, this strategy can also minimize the total number of HA constructs and enable incorporation of other antigenic components in the vaccine formulation. The three-dimensional (3D) structures and neutralizing epitopes of these cHAs were predicted and analyzed using structural bioinformatics and immunoinformatics approaches. Furthermore, a chimpanzee adenoviral vector (AdC68) was utilized to express these novel cHAs, later named as AdC68-cHAs. The immunogenicity and protective efficacy of AdC68-cHAs were then evaluated in a mouse model, and the results highlighted that AdC68-cH1-H7 elicited both H1 and H7 specific potent humoral immune response and protected mice from lethal challenges with both H1 and H7. Therefore, the innovative cHAs immunogen strategy reported in this study efficiently displayed protective antigens of two different head domains in one construct without loss of immunogenicity, which is the first study to devise such novel multi-HA head-based cHAs as immunogens.

Materials and methods

Cells and viruses

Human embryonic kidney 293 (HEK293) and Madin-Darby canine kidney (MDCK) cells were purchased from ATCC and cultured in Dulbecco's modified Eagle's medium (DMEM) (Gibco, Grand Island, NY, USA) supplemented with 10% fetal bovine serum (FBS) (Gibco) and 100 units/mL of penicillin and 100 g/mL of streptomycin at 37°C with 5% CO_2. The influenza virus pH1N1 (A/California/07/2009), seasonal H1N1 (A/Christchurch/16/2010 NIB-74), H7N9 (A/Shanghai/4664 T/2013), and H3N2 (A/Aichi/2/1968) were preserved in our laboratory. All influenza viruses were titrated using a 50% tissue culture infectious dose ($TCID_{50}$) assay on MDCK cells and median lethal dose 50 (LD_{50}) assay in C57BL/6 mice.

Constructions of recombinant adenoviruses

The HA genes of pandemic H1N1 (pH1N1) (A/California/07/2009), H3N2 (A/Aichi/2/1968), and H7N9 (A/

Zhejiang/DTID-ZJU01/2013) were downloaded from NCBI GenBank (accession number: KU933485.1, EF614248.1, KC885956.1) and synthesized by Gen-Script Biotech (Nanjing, China) after human codon optimization. Accordingly, a pair of conserved cysteines at positions 52 and 277 (H3 numbering) of HA was recognized as a demarcation line for the head/stalk interface of the influenza A virus [26, 27]. We then acquired the HA head domains from the influenza A virus pH1N1, H3N2, and H7N9 mentioned above.

To construct novel cHAs consisting of multiple head domains atop one stalk, sequential fusions containing two or three head domains were initially assembled. The head domains from H1 and H3 with a conserved pair of cysteines were fuzed by a flexible linker GGG (Gly–Gly–Gly) through overlap PCR and named H1-H3. Similarly, the head domains from H1 and H7 were also fuzed and named H1-H7. Moreover, H1-H3 was further fuzed with the head domain from H7 through the same method and named H1-H3-H7; H1-H7 was fuzed with the head domain from H3 and named H1-H7-H3. After that, the fuzed head domains were grafted onto the stalk domain derived from H1 via overlap PCR. Therefore, numerous novel cHAs consisting of multiple heads atop one stalk were attained, named cH1-H3, cH1-H7, cH1-H3-H7, and cH1-H7-H3, respectively. In addition, classical cHAs (cH3 and cH7) composed of a single head atop the H1 stalk were also constructed along with the H1 full-length HA to serve as controls.

To obtain recombinant adenoviruses expressing HA, the full-length HA of H1, classical cHAs (cH3, cH7), and novel cHAs (cH1-H3, cH1-H7, cH1-H3-H7, and cH1-H7-H3) were firstly cloned into the pShuttle plasmid (Clontech, San Francisco, USA) under the CMV promoter. Subsequently, the CMV-HA expression cassettes were respectively inserted into the E1 region of the adenoviral plasmid AdC68-empty which was generated in our lab [28]. The recombinant adenoviral plasmids AdC68-H1, AdC68-cH3, AdC68-cH7, AdC68-cH1-H3, AdC68-cH1-H7, AdC68-cH1-H3-H7, and AdC68-cH1-H7-H3 were then linearized with *Pac*I and transfected into HEK293 cells using Lipofectamine 2000 (Invitrogen, Carlsbad, CA, USA). When the recombinant adenoviruses were rescued, they were amplified in HEK293 cells and purified through CsCl density gradient ultracentrifugation.

Western blot

HEK293 cells were seeded in 6-well plates (1×10^6 cells/well). After 24 h, the cells were infected with different adenoviruses (AdC68-empty, AdC68-H1 AdC68-cH3, AdC68-cH7, AdC68-cH1-H3, AdC68-cH1-H7, AdC68-cH1-H3-H7, or AdC68-cH1-H7-H3) at a dose of 5×10^9 vp per well. After 24 h

post infection (hpi), all cells were harvested and washed twice with PBS and then incubated with RIPA lysis buffer containing proteinase inhibitors (Beyotime Biotechnology, Shanghai, China) on ice for 20 min. After centrifugation, the supernatant was harvested for Western blot analysis under reducing and non-reducing conditions. After sodium dodecyl sulfate (SDS)-polyacrylamide gel electrophoresis (PAGE), the proteins were transferred onto a PVDF membrane. The expression of cHAs was detected using antibodies against influenza pH1N1 (Sino Biological, Beijing, China, 11085-T54), H3N2 (Sino Biological, 11707-T38), or H7N9 (Sino Biological, 40104-RP02).

Structural modelling

The 3D structure of the cHAs was constructed via structure modelling, including monomer structure modelling and trimer structure construction. The monomer structures of cHAs were modelled using the online tools of Robetta, including the algorithms of RoseTTAFold [29]. Rosetta Comparative Modelling (CM) [30], and Ab Initio Modelling (AB) [31]. Among them, the parameters of CM were defined as models = 10, register shifts = 4, and fragments = 0.5, while the parameters of the other algorithms used the default settings for prediction. After prediction, the Robetta server provided the top five modelling structures and their corresponding confidence scores.

The trimer structures were constructed based on the corresponding monomer structures. Considering that all the cHAs shared the same stalk sequences of H1, the trimer structure of influenza A virus H1N1 (A/Netherlands/002P1/1951) derived from the PDB database (PDB ID: 6N41) [32] was selected as the template for model construction. The process of trimer structure simulation involved the transformation of residue coordinates. Specifically, the atomic coordinates of the stalk region of the monomer structure obtained from monomer structure modelling will be super-positioned with the atomic coordinates of the individual chain from the template trimer. Then, the residue coordinates of the other regions from the monomer structure will be transformed according to the same pattern. Here, we used the console mode of Pymol to achieve the above goal with the following steps.

Structure alignment

Three chains of the trimer structure were labelled in Pymol version 2.0 as chain A, chain B, and chain C. Then, the HA monomer was opened to align with chain A with the parameters extra_fit 1-3-7_MODEL_2, Chain A, method = align, cycles = 5,

cutoff = 2.0, mobile_state = −1, and target_state = −1. The RMSD score was then calculated for rational analysis in equation (1) as follows:

$$RMSD = \sqrt{\frac{\sum_{i=0}^{N}[(X_i - Y_i)^2]}{N}} \qquad (1)$$

where N is the number of considered atoms, X_i is the coordinate vector for the target atom i, and Y_i is the coordinate vector for the reference atom i. Here, we used the cutoff of RMSD < 0.5 Å and saved the object as new object 1 (new-obj1).

The above process was repeated for chain B and chain C from the same trimer structure to complete the construction of the new objects new-obj2 and new-obj3. After setting new-obj1 as the benchmark protein domain of the trimer structure, the other domains that completed the coordinate conversion can then be added to new-obj1 to generate a new trimer structure. The new trimer structure can be saved in the PSE file format for subsequent energy optimization. Finally, the energy-optimized structure can be saved as a new PDB structure for the cHA trimer.

Structure evaluation

To evaluate the rationality of the generated trimer structure model, the Ramachandran plot (RP) was introduced as the reference. The principle of the RP is based on the minimum contact distance between unbound atoms in a protein to determine whether the conformations of two adjacent peptide units defined by the pair-wise dihedral angles (Φ and Ψ) are allowed. Then, the RP is drawn by taking Φ as the horizontal coordinate and Ψ as the vertical coordinate. Here, the RP was generated using PDBsum [33]. From the coordinate plot, the protein structure can be divided into four regions: the most favoured regions (ABL), additional allowed regions (ablp), generously allowed regions (~a,~b,~l,~p), and disallowed regions (disallowed). When the total number of residues in the most favoured regions and other allowed regions reaches more than 90%, it indicates that the whole protein structure is a reasonable structure; otherwise, it is an unreasonable structure.

Epitope extraction

The epitope structures of HA from H1, H3 and H7 were extracted from the crystallized HA-antibody complex structures from Protein Data Bank [32], including the PDB ID of 4GXU, 4HKX, 5UGY, and 6ML8 for H1, 1KEN, 1QFU, 4FP8, 4GMS, 5UMU, and 4O58 for H3, 5VAG and 6II4 for H7, respectively. For each HA-antibody complex, epitope residues were

defined by the distance of the closest atom to antibody residues according to equation (2) as follows:

$$agr_i \in EpR, \text{ if } \exists A_j$$
$$\in agr_i \ \& \ D_{min}(agr_iA_j, \ AbRA) \leq 4 \text{ Å} \qquad (2)$$

where EpR represents the set of epitope residues if atom A_j is in antigen residue agr_i, meeting the condition that if the minimum distance between agr_iA_j and any atom from a corresponding antibody ($AbRA$) is less than 4 Å, then agr_i belongs to EpR. Finally, the epitope residues were mapped on the 3D structure of HA. For better illustration, nearby or highly overlapped epitopes were merged together, and three epitope regions were derived for H1, H3 and H7, respectively.

Calculation of SASA values

The SASA values were calculated using Naccess V2.1.1 [34]. Residues with a SASA value of more than 1 Å^2 can be considered surface residues. The SASA of each residue on the epitope regions can be calculated within the model of the trimer structures. The SASA of each epitope for different HAs was also calculated based on the original structures of H1 (PDB ID: 5XHV), H3 (PDB ID: 3VUN), and H7 (PDB ID: 4KOL) as benchmarks.

Animal experiments

All experiments were performed in accordance with the Animal Care and Use Committee of the Biosafety Committee of the Institut Pasteur of Shanghai (approval number: A2019038). Female C57BL/6 mice aged 6–8 weeks were bought from Vital River Laboratory (Beijing, China) and housed in the Biological Safety Level 2 laboratory of the Institut Pasteur of Shanghai. Experiments related to H7N9 were conducted in a biosafety level 3 laboratory following the standard operating protocols approved by the Institutional Biosafety Committee of the Shanghai Public Health Clinical Center, Fudan University.

The mice were divided into seven groups and immunized intramuscularly with different adenoviruses, including AdC68-empty, AdC68-H1, AdC68-cH7, and AdC68-cH1-H7 at a dose of 5×10^{10} vp (in 100 μL PBS) per mouse. At weeks 2, 4, and 6 post-vaccination, the mice were bled, and their sera were preserved at −80 °C until further analyses. Six weeks post-immunization, the mice were anesthetized intraperitoneally with 0.5% pentobarbital sodium (75 mg/kg) and then challenged intranasally with 10 LD$_{50}$ of different subtypes of influenza A virus (30 μL per mouse), including pH1N1 (A/California/07/2009), seasonal H1N1 (A/Christchurch/16/2010 NIB-74) or H7N9 (A/Shanghai/4664 T/2013). The body weight and survival of the mice were

monitored for 14 days post-challenge. Additionally, the mice were euthanized and defined dead when they lost more than 30% of their initial body weight.

Enzyme-linked immunosorbent assay (ELISA)

Briefly, 96-well plates (Corning, NY, USA) were coated with inactivated influenza virus pH1N1, seasonal H1N1, H7N9, or H3N2 HA protein (Sino Biological, 11707-V08B) at 4°C overnight. The plates were washed five times with PBS containing 0.5% Tween-20 (PBST) and then blocked with 5% skim milk (200 μL/well) for 2 h at 37°C. The inactivated mouse sera collected at week 4 were diluted in 1% skim milk (1:400) and added to each well. After incubation for 2 h at 37°C, the plates were washed with PBST and then incubated with HRP-conjugated goat anti-mouse IgG Fc (1:10000, 100 μL/well) for 1 h at 37°C. The substrate TMB (New Cell & Molecular Biotech Co., Ltd, Suzhou, China) was then added to each well and the reaction was stopped with 2 M sulfuric acid (H_2SO_4) solution (50 μL/well). The optical density was then read at 450 nm using a microtiter plate reader (Thermo Scientific, Waltham, MA).

HAI assay

The mouse sera collected at weeks 2, 4, and 6 post-immunization were mixed with receptor-destroying enzyme (RDE) from *Vibrio cholerae* (Denka Seiken) at 37°C overnight, and then heat-treated for 30 min at 56°C. After that, the sera were 2-fold serially diluted in PBS and incubated with 4 HA units of pH1N1, seasonal H1N1, H3N2, or H7N9 in equal volumes (25 μL) for 1 h at room temperature. Later, the mixture of serum and viruses (50 μL) was added to 96-well V-bottom plates, and 50 μL of 0.5% chicken red blood cells (RBCs) were added to each well. After 15 min of incubation at room temperature, the HAI titre was determined as the reciprocal of the highest dilution of serum that completely blocked RBC agglutination.

Microneutralization assay

MDCK cells were seeded in 96-well plates (1×10^4 cells/well) and cultured overnight. The inactivated mouse serum collected at weeks 2, 4, and 6 post-immunization were 2-fold serially diluted in a virus growth medium, comprising DMEM supplemented with 1% BSA, 100 U/mL of penicillin, 100 g/mL of streptomycin, and 2 μg/mL L-1-tosylamide-2-phenylethyl chloromethyl ketone (TPCK)-treated trypsin. The diluted serum was incubated with an equal volume of 100 $TCID_{50}$ of pH1N1, seasonal H1N1, H3N2, or H7N9 for 1 h at room temperature. The mixture of serum and viruses was then added to the MDCK cells, which were washed twice before the mixture was added. After 48 h of incubation at 37°C, 50 μL of the culture supernatant was added to each well of a 96-well V-bottom plate, and then 50 μL of 0.5% RBC was added to each well. After 15 min of incubation at room temperature, the neutralizing (NT) titre was determined as the reciprocal of the highest dilution of serum that completely blocked RBC agglutination.

Quantification of viral load in the lungs

The mice were euthanized on day 5 post-pH1N1 challenge. The lung tissues were collected, weighed, and then homogenized in 1 mL TRIzol reagent (Invitrogen, CA, USA). Total RNA was extracted and reverse-transcribed to cDNA using a One-Step RT–PCR Kit according to the manufacturer's protocol (Roche, Basel, Switzerland). After that, quantitative real-time PCR was conducted to determine the viral loads using specific primers of the M gene (Forward: 5′-AAGACCAATCCTGTCACCTCTGA-3′; Reverse: 5′-CAAAGCGTCTACGCTGCAGTCC-3′). The viral copies were expressed as the M gene copy number per 10 milligrams of the lung, which were calculated using a standard curve generated from a series of diluted pHW2000-M plasmids.

Histology

To examine the pathological changes in the lungs, lung tissues were first fixed in 4% formaldehyde. After 24 h of incubation at 4°C, the tissues were sent to a company for hematoxylin and eosin (H&E) staining, and the pathological damage was scored according to the following principles, as previously described [35]: 1, no observable pathology; 2, perivascular infiltrates; 3, perivascular and interstitial infiltrates affecting <20% of the lobe section; 4, perivascular and interstitial infiltrates affecting 20–50% of the lobe section; 5, perivascular and interstitial infiltrates affecting >50% of the lobe section. Five fields of each sample were randomly selected for score evaluation according to the principles above.

Statistical analysis

All statistical analyses were performed using GraphPad Prism software version 9.0. Significance was determined using one-way analysis of variance (ANOVA). Data are represented as the mean ± standard deviation (SD), wherein *, $P < 0.05$; **, $P < 0.01$; ***, $P < 0.001$; and ns, no significance.

Results

Construction and expression of novel cHAs

To construct novel cHAs, a conserved stalk domain derived from pandemic H1N1 (pH1N1) was used
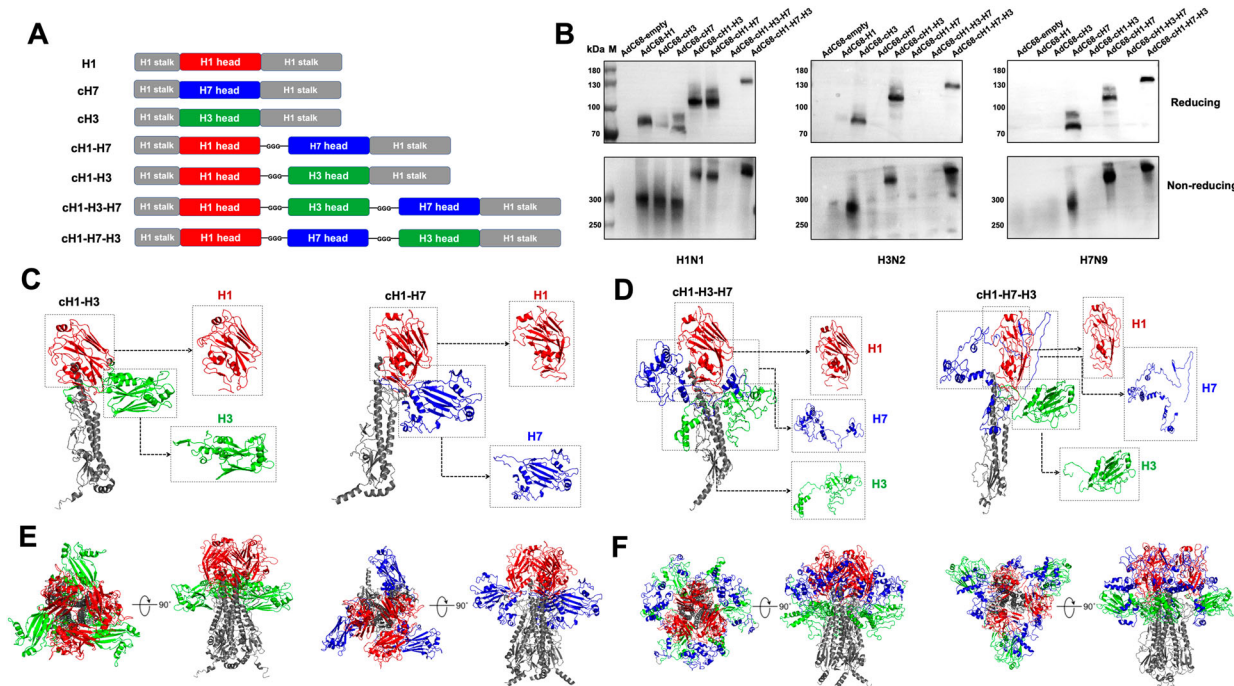
Figure 1. Construction, expression, and structural modelling of novel cHAs. (A) Schematic diagram of cHAs construction. The head domain from pH1N1 was linked with the head domains from H3N2 and H7N9 using the flexible linker Gly-Gly-Gly (GGG). The fuzed two or three head domains were then incorporated into the pH1N1 stalk and designated as cH1-H3, cH1-H7, cH1-H3-H7, or cH1-H7-H3. The full-length HA of pH1N1 and classical cHA, including cH3 and cH7, were also constructed as controls. The H1 stalk, H1 head, H3 head, and H7 head were marked in gray, red, green, and blue, respectively. **(B)** HEK293 cells were infected with the indicated adenoviruses. After 24 hpi, the cells were collected to detect the expression of cHAs via Western blotting using HA-specific anti-pH1N1, anti-H3N2, and anti-H7N9 polyclonal antibodies. **(C)** Monomer structures of cH1-H3 and cH1-H7. **(D)** Monomer structures of cH1-H3-H7 and cH1-H7-H3. **(E)** Trimer structures of cH1-H3 and cH1-H7 were shown in the vertical view and front view. **(F)** Trimer structures of cH1-H3-H7 and cH1-H7-H3 were shown in the vertical view and front view. The stalk, H1 head, H3 head, and H7 head were marked in gray, red, green, and blue, respectively.

as a scaffold. Initially, cHAs with two head domains on the top of the stalk were created by linking the head domain from pH1N1 with that of H3N2 or H7N9 using a flexible glycine linker (GGG). These fuzed head domains were then incorporated into the stalk of pH1N1 to generate cH1-H3 or cH1-H7. After that, three-headed cHAs (cH1-H3-H7 and cH1-H7-H3) were constructed by fuzing the H7 or H3 head domain with cH1-H3 or cH1-H7 in tandem, also through the GGG linker. A schematic was illustrated in Figure 1A. To produce adenoviral vector-based vaccines, the cHAs cH1-H3, cH1-H7, cH1-H3-H7, and cH1-H7-H3 were subcloned into a replication-deficient chimpanzee adenoviral vector (AdC68) to yield AdC68-cH1-H3, AdC68-cH1-H7, AdC68-cH1-H3-H7, and AdC68-cH1-H7-H3, respectively. In addition, control vectors were also constructed by subcloning the full-length HA of pH1N1 (H1) or the classical cHA expressing the pH1N1 stalk combined with the H3 or H7 head domain (cH3 or cH7, respectively) into AdC68, which were named AdC68-H1, AdC68-cH3, and AdC68-cH7, respectively.

To verify the expression of cHAs, HEK293 cells were infected with the above recombinant chimpanzee adenoviruses, including AdC68-H1, AdC68-cH3,

AdC68-cH7, AdC68-cH1-H3, AdC68-cH1-H7, AdC68-cH1-H3-H7, and AdC68-cH1-H7-H3, as well as the negative control virus AdC68-empty at a dose of 5×10^{9} virus particle (vp). After 24 h post infection (hpi), the cells were collected to perform Western blotting under reducing and non-reducing conditions. As depicted in Figure 1B, cHAs bands were detected in AdC68-cH1-H3-infected cells in both monomer and trimer forms when probed with anti-H1 or anti-H3 polyclonal antibodies, demonstrating that some epitopes of H1 and H3 can be concurrently expressed. Similarly, AdC68-cH1-H7 and AdC68-cH1-H7-H3 samples also showed cHAs bands when probed with the corresponding polyclonal antibodies. However, no cHAs bands were detected in the AdC68-cH1-H3-H7 sample; hence, we speculated that the order of the head domains might affect the conformation of the cHAs. Notably, the molecular weight of the cHAs in AdC68-cH1-H3, AdC68-cH1-H7, and AdC68-cH1-H7-H3 increased with an increasing number of head domains (in either monomer or trimer form) compared to AdC68-H1, AdC68-cH3, or AdC68-cH7. Overall, these results revealed that cHAs from AdC68-cH1-H3, AdC68-cH1-H7, and AdC68-cH1-H7-H3 were successfully expressed *in vitro*.

Structural simulation and analysis of the expressed cHAs

To further investigate the conformation of the expressed cHAs, we simulated the structures of cHAs using the Robetta server [29–31]. The monomer structures of cH1-H3, cH1-H7, cH1-H3-H7, and cH1-H7-H3 were shown in Figure 1C and D; and the trimer structures of these cHAs were shown in Figure 1E and F. After structural modelling, Ramachandran plots (RP) were built to evaluate the rationality of each modelled structure. Most of the residues in the modelled structures were found to locate in reasonable regions, as the most favoured regions (ABL) and additional allowed regions (ablp) could cover over 95.9% of the spaces in the RP (Supplement Table 1). Furthermore, structural simulation results showed that the stalk regions of all monomers could successfully form the secondary structures α-helices and β-sheets. The root-mean-square deviations (RMSDs) between the four monomer structures and the real PDB structure of the H1 stalk (template ID: 5K9O) ranged from 1.271–2.08 Å (Table 1), indicating that the stalk region could maintain almost the same conformational structure as the wild-type H1 HA stalk. Meanwhile, the results in this study showed that the H1 head domain in all four monomers could maintain structural integrity, and the RMSDs between the four monomer structures and the original H1 structure (PDB ID: 5XHV) ranged from 1.132 Å to 2.112 Å, which suggested that the H1 structure could maintain its complete spatial conformation as the backbone of the novel cHAs structure.

The cHAs of cH1-H3 and cH1-H7 were then analyzed for their structural similarity with the wild-type HA structure. Our results indicated that cH1-H7 possessed a structure very similar to the wild-type HA structure. The RMSD between the H7 head of cH1-H7 and the original H7 PDB structure (PDB ID: 4KOL) was only 2.707 Å, suggesting that its structural integrity was maintained, which may contribute to its good immunogenicity *in vivo*. In contrast, although the structural integrity of the H1 head in cH1-H3 was high (RMSD = 1.132 Å), the relatively high RMSD between the H3 head of cH1-H3 and the original H3 PDB structure (PDB ID: 3VUN; RMSD = 5.209 Å) demonstrated that the structural integrity of the H3 head in cH1-H3 was decreased, which could potentially reduce the immunogenicity of cH1-H3.

For the cHAs with three heads on one stalk (cH1-H3-H7 and cH1-H7-H3), significant damage was observed in the monomer and trimer structures, no matter the order of the HA head domain (Figure 1D, F). Specifically, the modelling results indicated that embedding three heads onto one stalk resulted in highly unstable structures, as evidenced by the large RMSDs between the simulated structures and the original PDB structures (22 and 29 Å for the H3 head and H7 head, respectively). Although the structure of the H1 and H3 heads in cH1-H7-H3 remained intact and shared a highly similar shape with the original PDB structure, the floating loop completely damaged their epitope presentations. Based on these findings, it was suggested that cHAs with three head domains atop one stalk might not be able to present the complete epitopes and stimulate immune responses *in vivo*.

Epitope mapping

Next, we analyzed the epitope exposure of the novel cHAs. Considering that the epitope region displayed on the monomer may be obscured in the trimer structure, we performed epitope mapping analysis based on the cHA trimeric structures (Figure 2). Using the crystallized HA-antibody complex structures from PDB, we extracted the epitopes from different structural isoforms and mapped them onto the templates of H1 (Figure 2A), H3 (Figure 2B), and H7 (Figure 2C) based on their spatial proximity. Since the cH1-H3-H7 and cH1-H7-H3 structures were incomplete or fragmented, epitope mapping analysis was only performed for cH1-H3 (Figure 2D) and cH1-H7 (Figure 2E). For each HA, three crystalized epitope regions were derived from the HA-antibody complexes and marked as H1-e1, H1-e2, H1-e3, H7-e1, H7-e2, H7-e3, H3-e1, H3-e2, and H3-e3. Compared with the classical epitope sites of H1, H1-e1 was a broadly protective epitope of antibody C179 [36]; H1-e2 contained the classical Ca2 epitope for H1 and H1-e3 contained the classical Sa/Sb epitope for H1 [37, 38]. Similarly, H3-e1 contained the classical H3 epitopes C and E; H3-e2 contained the classical H3 epitope A and H3-e3 contained the classical H3 epitopes B and D [39].

In the epitope mapping analysis of cH1-H3, it was observed that the epitopes H1-e2 and H1-e3 showed similar or greater exposure compared to the original H1 template, which led to the H3 head in cH1-H3 forming a different structural pattern from the H3 template, as evidenced by its RMSD being greater than 5 Å. For example, the H3-e1 epitope can be fully exposed in the original H3 trimer (solvent-accessible surface area [SASA] = 56.76 Å^2); however, it was covered in cH1-H3, with an 86% lower SASA of 7.97 Å^2. Meanwhile, H3-e2 and H3-e3 in cH1-H3 were both divided into two regions, failing to form complete epitope structures. For example, the amino acid

Table 1. RMSD between modelled structures and corresponding original PDB structures.

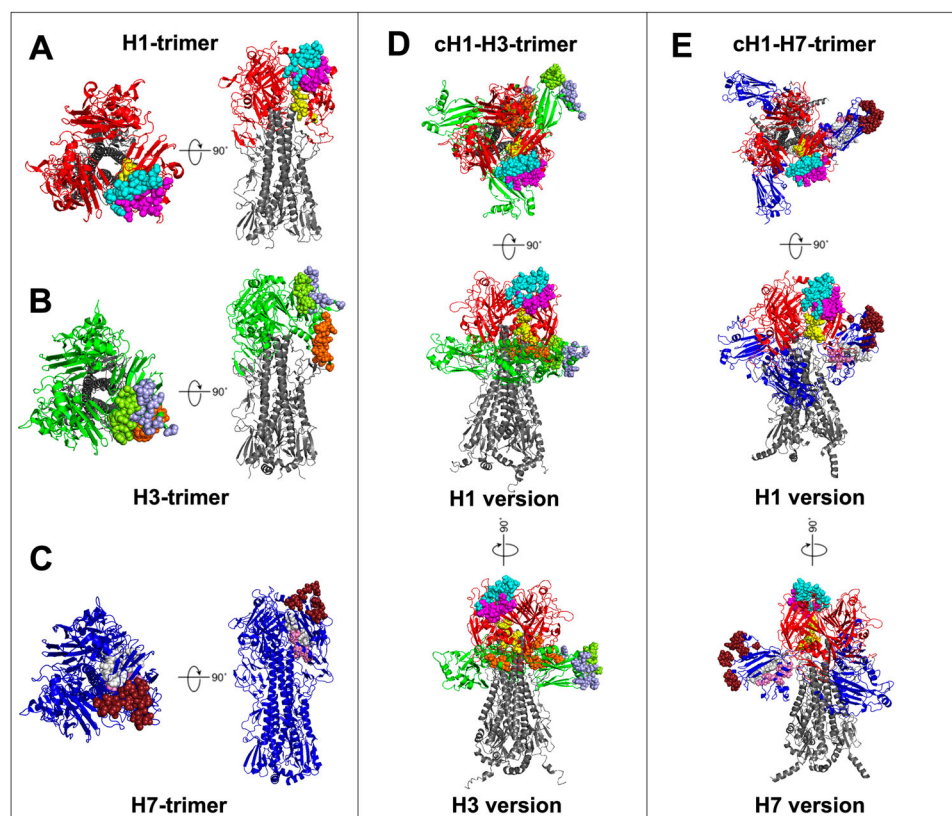| Structure domain	cH1-H3	cH1-H7	cH1-H3-H7	cH1-H7-H3
stalk	1,271 Å^2	1.574 Å^2	2.08 Å^2	1.497 Å^2
H1	1.132 Å^2	1.243 Å^2	1.643 Å^2	2.112 Å^2
H3	5.209 Å^2	—	22.098 Å^2	0.815 Å^2
H7	—	2.707 Å^2	22.36 Å^2	29.54 Å^2

Figure 2. Epitope mapping on cH1-H3 and cH1-H7. **(A)** Trimer structure for H1. The H1 head is marked in red, while the epitopes H1-e1, H1-e2, and H1-e3 are marked in yellow, magenta, and cyan, respectively. **(B)** Trimer structure for H3. The H3 head is marked in green, while the epitopes H3-e1, H3-e2, and H3-e3 are marked in orange, light blue, and limon, respectively. **(C)** Trimer structure for H7. The H7 head is marked in dark blue, while the epitopes H7-e1, H7-e2, and H7-e3 are marked in pink, ruby, and white, respectively. **(D)** Trimer structure of cH1-H3, with three versions of the vertical view, plan view (H1 version), and plan view with 90 degrees turning (H3 version). **(E)** Trimer structure for cH1-H7, with three versions of the vertical view, plan view (H1 version), and plan view with 90 degrees turning (H7 version). **(F)** Trimer structure for cH1-H7, with three versions of the vertical view, plan view (H1 version), and plan view with 90 degrees turning (H7 version).

96Y in the H3 trimer (labelled as 342Y in cH1-H3) can form a continuous spatial patch in H3-e2, while it remains an individual site in cH1-H3. Additionally, the H3 structure of cH1-H3 was found to block the H1 head from forming the "up" conformation, which resulted in a portion of the H1-e1 epitope being covered by the H3 structure, leading to the incomplete exposure of the H1-e1 epitope (Table 2). The incomplete exposure of H1-e1 and the disrupted H3 domain in cH1-H3 indicated that cH1-H3 might not exhibit diverse epitopes efficiently, potentially affecting its immunogenicity.

In contrast, in the epitope mapping analysis of cH1-H7, structural visualization illustrated that H1-e1,

H1-e2, H1-e3, H7-e1, H7-e2, and H7-e3 retained their complete epitope structures. Moreover, the H1-e1, H1-e2, and H1-e3 epitopes shared similar surface exposure patterns, with errors of less than 8% (for H1-e3). The epitopes H7-e1 and H7-e3 also shared similar surface exposure levels, with errors less than 7% (for H7-e3), while for H7-e2, the exposure level even increased by 15%, indicating enhanced exposure (Table 2). These epitope-mapping results demonstrated that both the H1 and H7 head domains in cH1-H7 formed complete structures and retained similar or increased epitope exposure than the original HA trimer.

Among the novel cHAs, the epitope-mapping analysis suggested that cH1-H7 could be a potent

Table 2. SASA of different epitopes on the trimer structure of original H1, original H3, original H7, cH1-H3 and cH1-H7.

Epitope	Color	H1	H3	H7	cH1-H3	cH1-H7
H1-e1	Yellow	25.021 Å²	–	–	10.854 Å²	25.015 Å²
H1-e2	Magenta	43.761 Å²	–	–	47.546 Å²	45.541 Å²
H1-e3	Cyan	60.373 Å²	–	–	69.173 Å²	65.247 Å²
H3-e1	Orange	–	56.76 Å²	–	56.76 Å²	–
H3-e2	Light Blue	–	53.19 Å²	–	53.19 Å²	–
H3-e3	Limon	–	57.76 Å²	–	57.76 Å²	–
H7-e1	Pink	–	–	37.41 Å²	–	37.36 Å²
H7-e2	Ruby	–	–	69.7 Å²	–	80.45 Å²
H7-e3	White	–	–	44.5 Å²	–	47.45 Å²

immunogen with the potential to induce effective immune responses *in vivo*, while cH1-H3 was not an ideal immunogen due to the disrupted structure of its epitopes.

Immunogenicity of AdC68-cHAs in mice

To evaluate the immunogenicity of AdC68-cHAs *in vivo*, C57BL/6 mice were immunized intramuscularly with AdC68-cH1-H3, AdC68-cH1-H7, or AdC68-cH1-H7-H3. Mice vaccinated with AdC68-empty, AdC68-H1, AdC68-cH3, or AdC68-cH7 were served as controls. As shown in Figure 3A, four weeks after immunization, ELISA was performed in the sera to determine the presence of binding antibodies against a panel of influenza viruses, including pH1N1, drifted seasonal H1N1, H3N2, and H7N9. Notably, similarly to the positive control group AdC68-H1, AdC68-cH1-H7 elicited specific binding antibody responses against pH1N1 and seasonal H1N1 (Figure 3B,C). Furthermore, AdC68-cH1-H7 also triggered binding
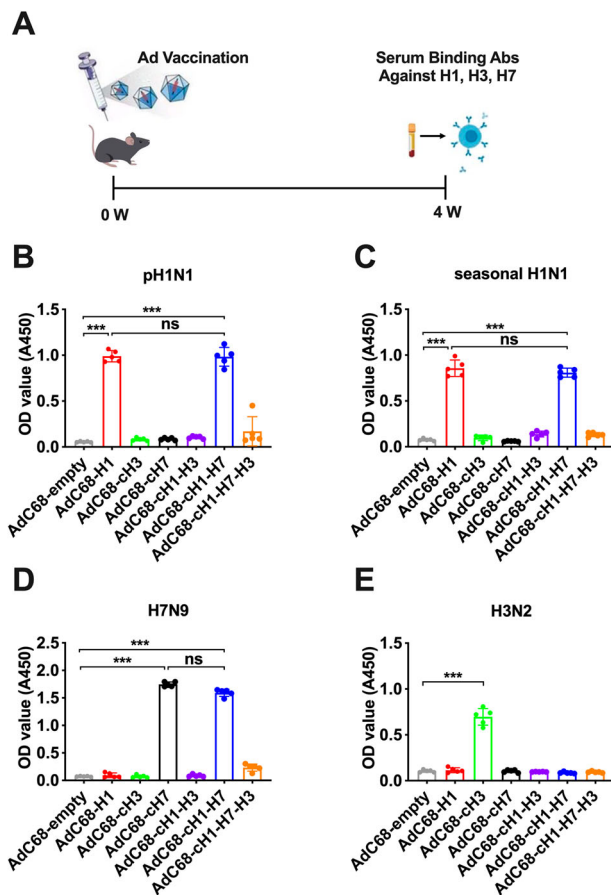
antibody responses against H7N9, of which the level was comparable to that of AdC68-cH7 (Figure 3D). The specific binding antibody response against H3N2 was only detected in AdC68-cH3 (Figure 3E), suggesting no cross-reaction was induced by any of two or three-headed cHAs. Distinct from AdC68-cH1-H7, AdC68-cH1-H3 or AdC68-cH1-H7-H3 failed to elicit antibody responses to any strains of the tested influenza viruses, possibly resulting from deficient structures or insufficient epitope exposure from the structural models shown in Figures 1 and 2.

Mice received a single vaccination of recombinant adenovirus with blood sampling fortnightly (Figure 4A). The neutralizing (NT) antibody responses were further analyzed (Figure 4B-E). AdC68-cH1-H7 group exhibited detectable NT antibody responses
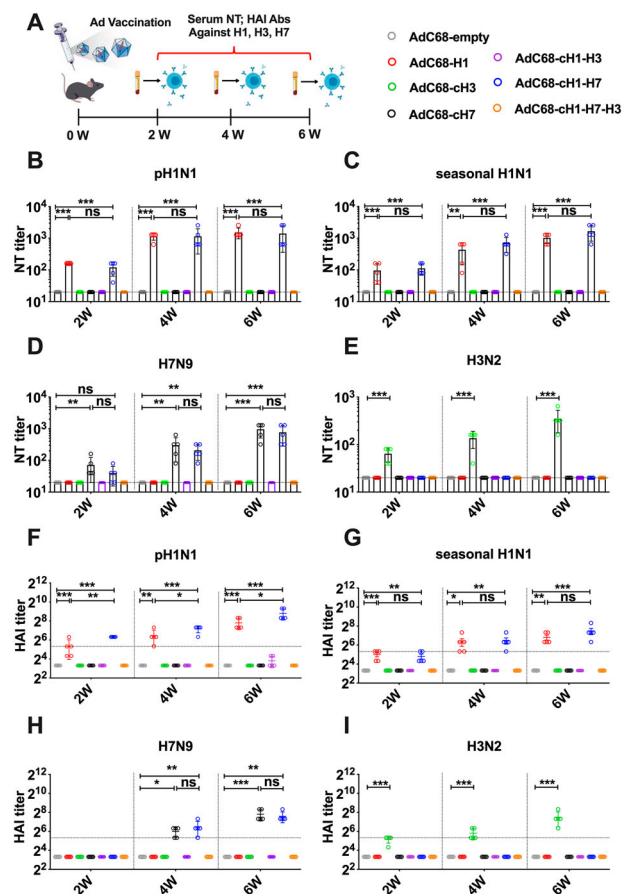

Figure 4. Neutralizing antibody and hemagglutination inhibition antibody responses of mice immunized with AdC68-cHAs. (A) The mice were intramuscularly vaccinated with the indicated adenoviruses. At 2, 4, and 6 weeks post-immunization, the mice were bled, and the levels of neutralizing (NT) antibodies and hemagglutination inhibition (HAI) antibodies in the serum against different subtypes of influenza virus were determined. (B-E) NT titres in the serum against pH1N1 (B), seasonal H1N1 (C), H7N9 (D), and H3N2 (E); horizontal dashed line represents limit of detection. (F-I) HAI titres in the serum against pH1N1 (F), seasonal H1N1 (G), H7N9 (H), and H3N2 (I); horizontal dashed line represents HAI titres equal to 40. Data are shown as the mean ± SD. Statistical significance was determined using one-way ANOVA. ns, no significance; *, $P < 0.05$; **, $P < 0.01$; ***, $P < 0.001$.

Figure 3. Binding antibody responses of mice immunized with AdC68-cHAs after 4 weeks. (A) Mice received a single vaccination of recombinant adenovirus. At 4 weeks post-immunization, the mice were bled to determine the binding antibody response against different influenza virus subtypes, including (B) pH1N1, (C) seasonal H1N1, (D) H7N9, and (E) H3N2 through ELISA. Data are shown as the mean ± SD. Statistical significance was determined using one-way ANOVA. ns, no significance; *, $P < 0.05$; **, $P < 0.01$; ***, $P < 0.001$.

against pH1N1, seasonal H1N1, and H7N9 at 2 weeks post-vaccination. At 6 weeks, the AdC68-cH1-H7 group showed even higher levels of NT antibodies, with geometric mean titres of 1408 (Figure 4B), 1664 (Figure 4C), and 768 (Figure 4D) against pH1N1, seasonal H1N1, and H7N9, respectively, which were equivalent to those induced by AdC68-H1 or AdC68-cH7. Consistent with the binding antibody responses, only AdC68-cH3 elicited a specific NT antibody response against H3N2 (Figure 4E). AdC68-cH1-H3 and AdC68-cH1-H7-H3 did not induce NT antibody responses against any strains of the tested influenza viruses, similar to the negative control, AdC68-empty.

The HAI antibody has been recognized to correlate with protection against influenza virus infection, of which titres over 40 could confer a 50% protective effect [40–43]. A similar tendency was observed in the HAI antibody responses as in the NT antibody responses (Figure 4F-I). Following AdC68-cH1-H7 vaccination, robust HAI antibody responses were concurrently induced against pH1N1, seasonal H1N1, and H7N9 with geometric mean titres of 448 (Figure 4F), 176 (Figure 4G), and 192 (Figure 4H) at 6 weeks, respectively. Importantly, the HAI antibody titres in mice in the AdC68-cH1-H7 group all greatly exceeded 40 at 6 weeks, suggesting that potent and comprehensive HAI responses were successfully elicited post-vaccination. In contrast, AdC68-cH1-H3 and AdC68-cH1-H7-H3 failed to induce HAI antibody responses to the tested influenza virus strains.

Overall, in line with the structural modelling and epitope mapping analysis of the cHAs, AdC68-cH1-H7 was highly immunogenic in mice, which elicited binding, NT, and HAI antibody responses against multiple strains of influenza virus, including pH1N1, drifted seasonal H1N1, and H7N9.

Protection against challenges with multiple strains of influenza virus

As AdC68-cH1-H7 demonstrated robust immunogenicity, the authenticity of its protective effectiveness was further evaluated. Mice were intramuscularly immunized with the AdC68-empty, AdC68-H1, AdC68-cH7, or AdC68-cH1-H7 and challenged with 10 LD_{50} of influenza A virus (Figure 5A), including pH1N1 (A/California/07/2009), seasonal H1N1 (A/Christchurch/16/2010 NIB-74), and H7N9 (A/Shanghai/4664 T/2013) at 6 weeks post-vaccination. The body weight and survival of the mice were monitored daily for 14 days following the lethal infection. The results demonstrated that AdC68-cH1-H7 provided 100% protection as AdC68-H1 against lethal challenges of pH1N1 and seasonal H1N1 with minimal to no weight loss observed (Figure 5B-E). In contrast, all mice in the AdC68-cH7 and negative control groups (AdC68-empty) exhibited severe weight loss
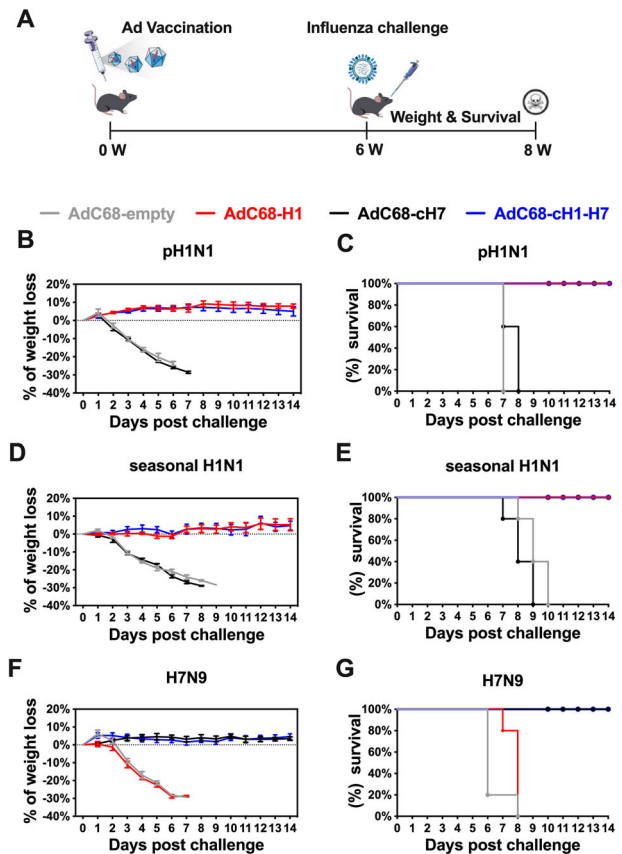

Figure 5. Protection efficacy elicited by AdC68-cH1-H7 against lethal challenges of multiple subtypes of influenza virus in vivo. (A) The mice were intranasally challenged with 10 LD_{50} of multiple subtypes of influenza virus at 6 weeks post-immunization. The body weight change and survival were recorded for 14 days after pH1N1 (B, C), seasonal H1N1 (D, E), and H7N9 (F, G) challenge. Body weight was presented as the mean ± SD.

and succumbed to infection within 10 days. Following H7N9 infection, no weight loss was observed in the AdC68-cH1-H7-vaccinated and AdC68-cH7-vaccinated groups, and all mice survived, indicating that AdC68-cH1-H7 also conferred 100% protection against lethal challenge of H7N9 virus (Figure 5F,G).

Analysis of pulmonary pathology and viral load post-pH1N1 challenge

To further investigate the pathological changes in the lungs, mice were challenged with 10 LD_{50} of pH1N1 and euthanized on day 5 post infection (dpi) (Figure 6A). Afterward, the lung tissues were collected for pathological evaluation and detection of viral loads. Mice that were vaccinated with AdC68-H1 or AdC68-cH1-H7 showed milder lung lesions, characterized by intact pulmonary alveoli, and reduced infiltration of inflammatory cells, which resulted in significantly lower pathological scores when compared to the AdC68-cH7-treated or negative control groups (Figure 6B,C). These observations were mainly attributed to the high levels of serological NT and HAI antibodies
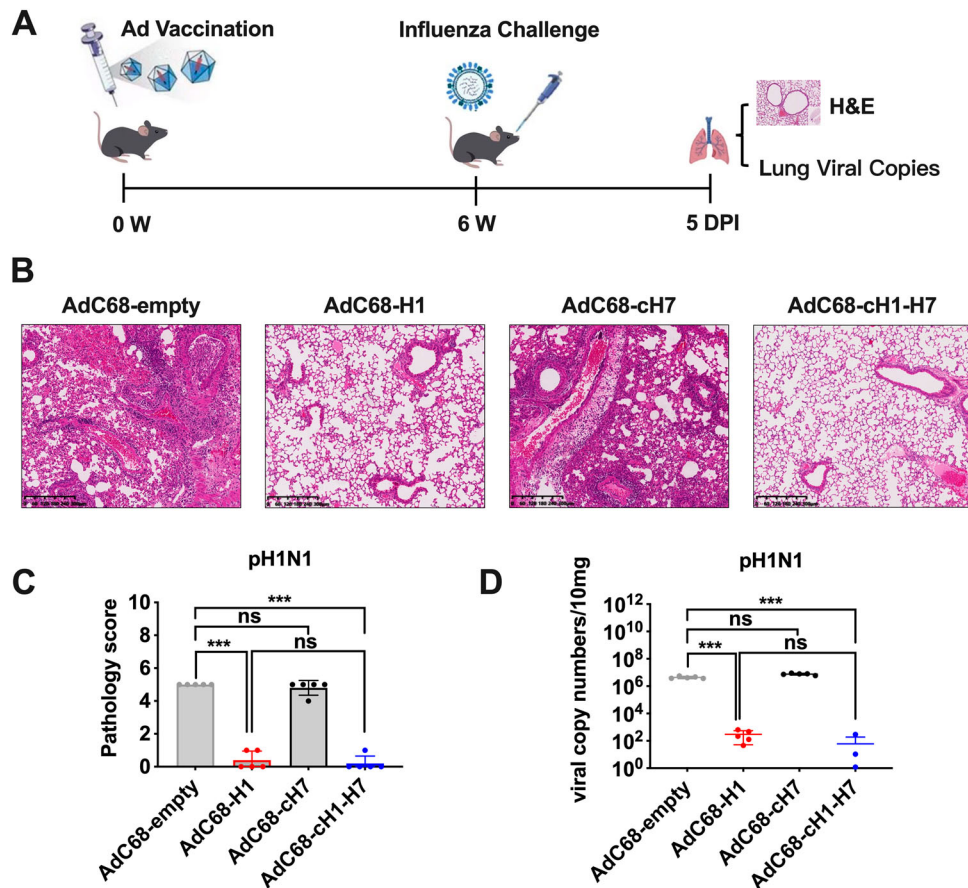
Figure 6. Lung pathological changes and viral load of mice challenged with pH1N1. (A) The mice were intranasally challenged with 10 LD_{50} of pH1N1 at 6 weeks post-immunization. On day 5 post infection (DPI), all mice were sacrificed, and the lungs were collected, which were used for **(B)** H&E staining, **(C)** pathology score evaluation, and **(D)** viral copies detection. Data were shown as the mean ± SD. Statistical significance was determined using one-way ANOVA. ns, no significance; *, $P < 0.05$; **, $P < 0.01$; ***, $P < 0.001$.

against pH1N1 in these mice. In contrast, all lungs from mice vaccinated with the AdC68-cH7 or AdC68-empty exhibited severe interstitial pneumonia, pulmonary alveolitis, and diffuse inflammatory cell infiltration, resulting in higher pathological scores. Moreover, the viral copies in the lungs of mice of the AdC68-cH1-H7 or AdC68-H1 groups decreased ∼10,000-fold compared to those treated with the AdC68-empty or AdC68-cH7. These results demonstrate that AdC68-cH1-H7 could significantly reduce the viral infection and thus efficiently protect mice from lethal pH1N1 challenge as AdC68-H1 (Figure 6D).

Discussion

The HA has been the primary target of influenza virus vaccines owing to its ability to induce efficient protection via virus neutralization, hemagglutination inhibition, and Fc effector functions [44–47]. To further broaden the protective efficacy of HA in this study, we proposed a new design for HA called cHAs and delivered various cHAs through a chimpanzee adenoviral vector. Here, the results showed that one of the novel cHAs, cH1-H7, demonstrated excellent immunogenicity in mice. Specifically, a single vaccination

with AdC68-cH1-H7 induced robust humoral responses and conferred complete protection against homologous pH1N1, drifted seasonal H1N1, and H7N9. Furthermore, reduced viral loads and relatively milder pathological damage were observed in the lungs of the AdC68-cH1-H7 group post-pH1N1 challenge compared to those treated with other recombinant adenoviruses. The success of the cH1-H7 immunogen solidifies the rationale that combining multiple individual HA head domains to form cHAs could ultimately enhance the breadth of immune responses.

The strategies to fuze H1 and H7 head domains as chimera may maximize and shape cross-reactive antibody responses against target epitopes. Kanekiyo et al. [48] found that co-displaying eight different HA head domains from diverse H1 strains on a single nanoparticle (NP) was able to elicit broader antibody responses compared to those induced by a "cocktail" immunogen containing equimolar amounts of individual HA-displaying nanoparticles. Moreover, a monoclonal antibody induced by this heterotypic mosaic NP was identified to broadly neutralize H1N1 viruses spanning over 90 years. Consistently, a recent study by Kang et al. [49] also reported that a mosaic NP presenting spike antigens from SARS-CoV-2 prototype

and three major variants (including Alpha, Beta, and Gamma variants) demonstrated a slight but stable preponderance over the cocktail NP in antibody responses against multiple SARS-CoV-2 variants. The mechanisms of the aforementioned results were proposed that the heterotypic mosaic antigen array was able to selectively activate cross-reactive B cells by offering a higher affinity advantage when the antigen-binding regions of the B cell receptor can recognize multiple antigen specificities, while a simple admixture of heterotypic immunogens failed to achieve such effect on account of separate distribution and presentation of antigens. Thus, we reasoned that the epitopes of H1 and H7 presented simultaneously as a chimera may make the antigenic sites accessible to B cells and create an opportunity for cross-reactive antibody responses between diverse antigens, which was thus superior to those mixed simply or expressed separately in eliciting cross-reactive B cell response. However, this hypothesis will require further investigation in our next study.

Unfortunately, despite the detection of the cH1-H3 and cH1-H7-H3 cHAs *in vitro*, AdC68-cH1-H3 or AdC68-cH1-H7-H3 failed to induce NT or HAI antibody responses to any strains of tested influenza virus. The poor immunogenicity of these cHAs *in vivo* may be due to the interactions of their head domains, which affected the conformation of cHAs and limited the exposure of key antigenic sites to the immune system. Nevertheless, bioinformatic structure analysis indicated that cH1-H7 retained the immunogenicity of H1 and H7 concurrently. The *in vivo* results further confirmed that, compared to vaccination with AdC68 encoding a single HA antigen (AdC68-H1 or AdC68-cH7 control), no substantial differences in the magnitude of humoral immune responses against H1 or H7 were detected in mice administrated with AdC68-cH1-H7. Thus, the rational optimization for cHAs remains to be conducted.

Immunity against adenoviral vectors is a concern, particularly when repeated vaccination of the same vector is applied. In a study by Sayedahmed *et al.* [50], mice were primed with AdHu5 and subsequently vaccinated with AdHu5-H5HA (AdHu5 vector expressing the HA of H5N1) at 1, 3, 6, or 10 months after the initial intramuscular inoculation. Results showed a decline in the neutralizing titres against the AdHu5 vector over time. However, there was a significant progressive increase in the levels of humoral and cellular immune responses against H5N1, demonstrating that annual vaccination with an influenza virus vaccine based on the same adenoviral vector may be viable. Additionally, the outbreak of an emerging influenza virus requires the production and delivery of vaccines to be convenient, efficient, and rapid. Adenoviral vector-based vaccines can be considered as alternative platforms for rapid production and efficient delivery through mucosal vaccination. The current licensed COVID-19 vaccine based on AdHu5 [51–53] has demonstrated superior protective immunity in inducing widespread protection spanning both mucosal and systemic immunity to limit virus infection and transmission. Of note, the cHAs may likely provide only sub-type or strain-specific protection based on the antibody response; while given the capacity of adenoviral vectors for delivering large amounts of transgenes [54], immune responses induced by AdC68-cH1-H7 can be further enhanced by arming divergent conserved antigens such as NA, M2e, or NP in the deleted E3 region, resulting in broader and more robust humoral and cellular responses against the influenza virus.

In summary, the success of AdC68-cH1-H7 demonstrated that more than one HA head domain could be combined with a stalk domain without loss of immunogenicity. To our knowledge, this is the first study to devise such novel multi-HA head-based cHAs as immunogens, which deserves further investigation as an alternative strategy to develop influenza virus vaccines.

The current study has several limitations that require further investigation. Obtaining accurate crystal structures containing multiple loop regions is conventionally arduous, making the structural analysis in this study reliant upon structural bioinformatics. However, crystal structures would provide more compelling evidence for the structural integrity and display patterns of the designed novel cHAs. The assessment of AdC68-cHAs has primarily focused on antibody response efficiency and protective outcomes, while cellular responses, especially the contributions of $CD4^+$ T and $CD8^+$ T cells, remain insufficiently explored. In the future, the purification of cHAs proteins and exploration of general rules for cHAs design will be quintessential to effectively design optimal cHAs that can provide broad-spectrum protection.

Author contributions

D.Z. and J.X. conceived the project and designed the experiments. P. Z., X.W., X.Y., H.S., C.Z., and W.D. performed the experiments. T.Q. conducted the structure modelling analysis. D.Z, P.Z., J.X., X.Z., and M.X. analyzed the data. P.Z. and T.Q. wrote the manuscript. D.Z. revised the manuscript.

Disclosure statement

Funding

References

[1] Kim Y-H, Hong K-J, Kim H, et al. Influenza vaccines: past, present, and future. Rev Med Virol. 2022;32(1): e2243.

[2] Iacobucci G. Covid-19: Risk of death more than doubled in people who also had flu, English data show. Br Med J. 2020;370:m3720.

[3] Yue H, Zhang M, Xing L, et al. The epidemiology and clinical characteristics of co-infection of SARS-CoV-2 and influenza viruses in patients during COVID-19 outbreak. J Med Virol. 2020;92(11):2870–2873.

[4] Chiu C. Seasonal influenza vaccines and hurdles to mutual protection. Clin Microbiol Infect. 2016;22 (Suppl 5):S113–S119.

[5] Berlanda Scorza F, Tsvetnitsky V, Donnelly JJ. Universal influenza vaccines: shifting to better vaccines. Vaccine. 2016;34(26):2926–2933.

[6] Heikkinen T, Ikonen N, Ziegler T. Impact of influenza B lineage-level mismatch between trivalent seasonal influenza vaccines and circulating viruses, 1999-2012. Clin Infect Dis. 2014;59(11):1519–1524.

[7] Pica N, Palese P. Toward a universal influenza virus vaccine: prospects and challenges. Annu Rev Med. 2013;64:189–202.

[8] Wei C-J, Crank MC, Shiver J, et al. Next-generation influenza vaccines: opportunities and challenges. Nat Rev Drug Discov. 2020;19(4):239–252.

[9] Stevens J, Corper AL, Basler CF, et al. Structure of the uncleaved human H1 hemagglutinin from the extinct 1918 influenza virus. Science. 2004;303(5665):1866–1870.

[10] Janssens Y, Joye J, Waerlop G, et al. The role of cell-mediated immunity against influenza and its implications for vaccine evaluation. Front Immunol. 2022;13:959379.

[11] Jegaskanda S, Andrews SF, Wheatley AK, et al. Hemagglutinin head-specific responses dominate over stem-specific responses following prime boost with mismatched vaccines. JCI Insight. 2019;4(22).

[12] Ermler ME, Kirkpatrick E, Sun W, et al. Chimeric hemagglutinin constructs induce broad protection against influenza B virus challenge in the mouse model. J Virol. 2017;91(12).

[13] Krammer F, Pica N, Hai R, et al. Chimeric hemagglutinin influenza virus vaccine constructs elicit broadly protective stalk-specific antibodies. J Virol. 2013;87 (12):6542–6550.

[14] Margine I, Krammer F, Hai R, et al. Hemagglutinin stalk-based universal vaccine constructs protect against group 2 influenza A viruses. J Virol. 2013 Oct;87(19):10435–10446.

[15] Ramasamy MN, Minassian AM, Ewer KJ, et al. Safety and immunogenicity of ChAdOx1 nCoV-19 vaccine administered in a prime-boost regimen in young and old adults (COV002): a single-blind, randomised, controlled, phase 2/3 trial. Lancet. 2021;396(10267):1979–1993.

[16] Voysey M, Clemens C, Madhi SA, et al. Single-dose administration and the influence of the timing of the booster dose on immunogenicity and efficacy of ChAdOx1 nCoV-19 (AZD1222) vaccine: a pooled analysis of four randomised trials. Lancet. 2021;397 (10277):881–891.

[17] Barnes E, Folgori A, Capone S, et al. Novel adenovirus-based vaccines induce broad and sustained T cell responses to HCV in man. Sci Transl Med. 2012;4(115):115ra1.

[18] Colloca S, Barnes E, Folgori A, et al. Vaccine vectors derived from a large collection of simian adenoviruses induce potent cellular immunity across multiple species. Sci Transl Med. 2012;4(115):115ra2.

[19] Peruzzi D, Dharmapuri S, Cirillo A, et al. A novel chimpanzee serotype-based adenoviral vector as delivery tool for cancer vaccines. Vaccine. 2009;27 (9):1293–1300.

[20] Quinn KM, Da Costa A, Yamamoto A, et al. Comparative analysis of the magnitude, quality, phenotype, and protective capacity of simian immunodeficiency virus gag-specific CD8+ T cells following human-, simian-, and chimpanzee-derived recombinant adenoviral vector immunization. J Immunol. 2013;190(6):2720–2735.

[21] Xu K, An Y, Li Q, et al. Recombinant chimpanzee adenovirus AdC7 expressing dimeric tandem-repeat spike protein RBD protects mice against COVID-19. Emerg Microbes Infect. 2021;10(1):1574–1588.

[22] Aartse A, Eggink D, Claireaux M, et al. Influenza A virus hemagglutinin trimer, head and stem proteins identify and quantify different hemagglutinin-specific B cell subsets in humans. Vaccines (Basel). 2021 Jul 2;9(7).

[23] McCarthy KR, Lee J, Watanabe A, et al. A prevalent focused human antibody response to the influenza virus hemagglutinin head interface. mBio. 2021 Jun 29;12(3):e0114421.

[24] Bangaru S, Lang S, Schotsaert M, et al. A site of vulnerability on the influenza virus hemagglutinin head domain trimer interface. Cell. 2019 May 16;177 (5):1136–1152 e18.

[25] Dong J, Gilchuk I, Li S, et al. Anti-influenza H7 human antibody targets antigenic site in hemagglutinin head domain interface. J Clin Invest. 2020 Sep 1;130 (9):4734–4739.

[26] Chen C-J, Ermler ME, Tan GS, et al. Influenza A viruses expressing intra- or intergroup chimeric hemagglutinins. J Virol. 2016;90(7):3789–3793.

[27] Hai R, Krammer F, Tan GS, et al. Influenza viruses expressing chimeric hemagglutinins: globular head and stalk domains derived from different subtypes. J Virol. 2012;86(10):5774–5781.

[28] Yang Y, Chi Y, Tang X, et al. Rapid, efficient, and modular generation of adenoviral vectors via isothermal assembly. Curr Protoc Mol Biol. 2016;113(1).

[29] Baek M, DiMaio F, Anishchenko I, et al. Accurate prediction of protein structures and interactions using a three-track neural network. Science. 2021;373 (6557):871–876.

[30] Song Y, DiMaio F, Wang RY-R, et al. High-resolution comparative modeling with RosettaCM. Structure. 2013;21(10):1735–1742.

[31] Raman S, Vernon R, Thompson J, et al. Structure prediction for CASP8 with all-atom refinement using Rosetta. Proteins. 2009;77(Suppl 9):89–99.

[32] Berman HM, Westbrook J, Feng Z, et al. The protein data bank. Nucleic Acids Res. 2000;28(1):235–242.

[33] de Beer TAP, Berka K, Thornton JM, et al. PDBsum additions. Nucleic Acids Res. 2014;42(Database issue):D292–D296.

[34] Hubbard SJ, Thornton JM, Campbell SF. Substrate recognition by proteinases. Faraday Discuss. 1992;93:13–23.

[35] Song Y, Wang X, Zhang H, et al. Repeated low-dose influenza virus infection causes severe disease in mice: a model for vaccine evaluation. J Virol. 2015;89(15):7841–7851.

[36] Yassine HM, Boyington JC, McTamney PM, et al. Hemagglutinin-stem nanoparticles generate hetero-subtypic influenza protection. Nat Med. 2015;21(9):1065–1070.

[37] Caton AJ, Brownlee GG, Yewdell JW, et al. The antigenic structure of the influenza virus A/PR/8/34 hemagglutinin (H1 subtype). Cell. 1982;31(2 Pt 1):417–427.

[38] Xu R, Ekiert DC, Krause JC, et al. Structural basis of preexisting immunity to the 2009 H1N1 pandemic influenza virus. Science. 2010;328(5976):357–360.

[39] Wiley DC, Wilson IA, Skehel JJ. Structural identification of the antibody-binding sites of Hong Kong influenza haemagglutinin and their involvement in antigenic variation. Nature. 1981;289(5796):373–378.

[40] Coudeville L, Bailleux F, Riche B, et al. Relationship between haemagglutination-inhibiting antibody titres and clinical protection against influenza: development and application of a bayesian random-effects model. BMC Med Res Methodol. 2010;10:18.

[41] Fox JP, Cooney MK, Hall CE, et al. Influenzavirus infections in Seattle families, 1975-1979. II. Pattern of infection in invaded households and relation of age and prior antibody to occurrence of infection and related illness. Am J Epidemiol. 1982;116(2):228–242.

[42] McCullers JA, Huber VC. Correlates of vaccine protection from influenza and its complications. Hum Vaccin Immunother. 2012;8(1):34–44.

[43] Ng S, Fang VJ, Ip DKM, et al. Estimation of the association between antibody titers and protection against confirmed influenza virus infection in children. J Infect Dis. 2013;208(8):1320–1324.

[44] He W, Tan GS, Mullarkey CE, et al. Epitope specificity plays a critical role in regulating antibody-dependent cell-mediated cytotoxicity against influenza A virus. Proc Natl Acad Sci U S A. 2016;113(42):11931–11936.

[45] Henry Dunand CJ, Leon PE, Huang M, et al. Both neutralizing and non-neutralizing human H7N9 influenza vaccine-induced monoclonal antibodies confer protection. Cell Host Microbe. 2016;19(6):800–813.

[46] Kirchenbaum GA, Ross TM. Eliciting broadly protective antibody responses against influenza. Curr Opin Immunol. 2014;28:71–76.

[47] Tan GS, Leon PE, Albrecht RA, et al. Broadly-reactive neutralizing and non-neutralizing antibodies directed against the H7 influenza virus hemagglutinin reveal divergent mechanisms of protection. PLoS Pathog. 2016;12(4):e1005578.

[48] Kanekiyo M, Joyce MG, Gillespie RA, et al. Mosaic nanoparticle display of diverse influenza virus hemagglutinins elicits broad B cell responses. Nat Immunol. 2019;20(3):362–372.

[49] Kang YF, Sun C, Sun J, et al. Quadrivalent mosaic HexaPro-bearing nanoparticle vaccine protects against infection of SARS-CoV-2 variants. Nat Commun. 2022 May 13;13(1):2674.

[50] Sayedahmed EE, Kumari R, Shukla S, et al. Longevity of adenovirus vector immunity in mice and its implications for vaccine efficacy. Vaccine. 2018;36(45):6744–6751.

[51] Halperin SA, Ye L, MacKinnon-Cameron D, et al. Final efficacy analysis, interim safety analysis, and immunogenicity of a single dose of recombinant novel coronavirus vaccine (adenovirus type 5 vector) in adults 18 years and older: an international, multi-centre, randomised, double-blinded, placebo-controlled phase 3 trial. Lancet. 2022;399(10321):237–248.

[52] Wu S, Huang J, Zhang Z, et al. Safety, tolerability, and immunogenicity of an aerosolised adenovirus type-5 vector-based COVID-19 vaccine (Ad5-nCoV) in adults: preliminary report of an open-label and randomised phase 1 clinical trial. Lancet Infect Dis. 2021;21(12):1654–1664.

[53] Zhu F-C, Guan X-H, Li Y-H, et al. Immunogenicity and safety of a recombinant adenovirus type-5-vectored COVID-19 vaccine in healthy adults aged 18 years or older: a randomised, double-blind, placebo-controlled, phase 2 trial. Lancet. 2020;396(10249):479–488.

[54] Sakurai F, Tachibana M, Mizuguchi H. Adenovirus vector-based vaccine for infectious diseases. Drug Metab Pharmacokinet. 2022;42:100432.